

The [Fe XIII] Infrared 10747Å and 10798Å Lines in Novae

D. P. K. BANERJEE ,¹ C. E. WOODWARD ,² A. EVANS ,³ T. R. GEBALLE ,⁴ V. JOSHI ,¹ AND S. STARRFIELD ,⁵

¹Physical Research Laboratory, Navrangpura, Ahmedabad, Gujarat 380009, India

²Minnesota Institute for Astrophysics, School of Physics & Astronomy, 116 Church Street SE, University of Minnesota, Minneapolis, MN 55455, USA

³Astrophysics Research Centre, Lennard Jones Laboratory, Keele University, Keele, Staffordshire, ST5 5BG, UK

⁴Gemini Observatory/NSF's NOIRLab, 670 N. Aohoku Place, Hilo, HI, 96720, USA

⁵School of Earth and Space Exploration, Arizona State University, Box 876004, Tempe, AZ 85287-6004, USA

(Received 2025 Dec 14; Revised 2026 Jan 19; Accepted 2026 Jan 19)

ABSTRACT

The forbidden lines of [Fe XIII] at 10747Å and 10798Å are among the most prominent lines in the near-infrared spectrum of the solar corona. They have been used routinely, both outside and during eclipses, as sensitive probes of the electron density and polarization in the solar corona. Many novae pass through a coronal phase, wherein the highly ionized nova ejecta have physical conditions that are remarkably similar to those of the solar corona. Many of the coronal emission lines that are seen are common to the spectra of both the Sun and novae. Yet, it appears that no robust detection of the [Fe XIII] lines has been made in a nova. Here we report the detection of these two infrared [Fe XIII] lines in the spectrum of the recurrent nova V3890 Sgr, taken 23.43 and 31.35 days after its August 2019 outburst. From their line strengths, we derive values of 10^{10} cm $^{-3}$ and $10^{[8.5-9]}$ cm $^{-3}$ for the electron density on the two epochs. The decrease in density between epochs can be explained if the density decreased with a power law $n(r) \propto r^\alpha$, with a α inferred to be -3 . The average temperature of the coronal gas is estimated to be $T = (2.51 \pm 0.06) \times 10^6$ K. We find that recurrent novae with giant secondaries, including T CrB whose eruption is imminent, are the most suitable sources for further detections of the [Fe XIII] lines.

Keywords: Stellar coronal lines (308) – Circumstellar gas (238) – Near infrared astronomy (1093) – Novae (1127) – Recurrent novae (1366) – Infrared spectroscopy (2285)

1. INTRODUCTION

The presence of bright emission lines in the corona have been observed during total solar eclipses since the 19th century, the most prominent being the “green line” (Fe XIV at 5303Å)¹, possibly first observed in 1869. With the invention of the coronagraph in the 1930s (B. Lyot 1939), these lines could be observed even outside of eclipses. Lyot observed numerous coronal lines at Pic-du-Midi, discovering the near-infrared 10747Å and 10798Å lines in 1936, for which he employed hypersensitization techniques to increase the sensitivity of photographic plates to infrared radiation. The lines were eventually identified by B. Edlén (1945), and shown to be forbidden transitions of Fe XIII. The lines are

forbidden magnetic dipole (M1) transitions, and come from very hot regions of the corona. The effective temperature at which Fe XIII has its maximum ionization fraction is $T_{\text{eff}} = 1.8 \times 10^6$ K ($\log T_{\text{eff}} = 6.25$; T. A. Schad et al. 2023). The ionization potential of Fe XII is 330.8 eV.

The two lines arise from different upper levels, as shown in Figure 1. They are a useful diagnostic to determine the electron density and temperature, as well as for magnetometry. In the latter context, there are a number of suitable forbidden lines in the solar corona (e.g., [Fe XV] 5303Å, [Fe X] 6374Å, [Fe XIII] 10750Å). Measurement of the full Stokes vectors of these lines can give information on the magnetic field properties. Indeed the magnetic sensitivity of the [Fe XIII] 10747Å line is significantly higher than lines in the visible, because of Zeeman splitting, $\Delta\lambda \propto \lambda^2 B$.

The 10747Å line is one of the strongest solar corona emission lines in the near-infrared, and is widely used for

Corresponding author: C.E. Woodward

Email: dpkb12345@gmail.com, chickw024@gmail.com

¹ All wavelengths are in air.

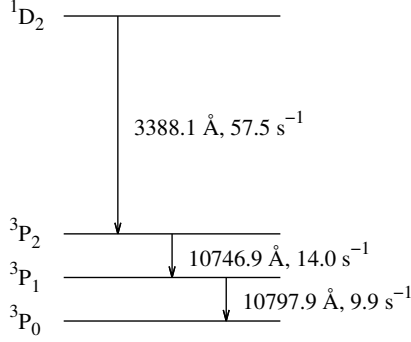


Figure 1. Term diagram for the [Fe XIII] lines of interest. The transition probabilities are shown to the right of the wavelengths. The 3P_2 and 3P_1 are 1.15 eV and 2.301 eV above the ground state respectively. Transition probabilities taken from NIST database <https://physics.nist.gov/PhysRefData/ASD/lines-form.html>

solar coronal analysis. However in novae, the [Fe XIII] lines have not been detected, except perhaps in the extragalactic recurrent nova M31-2008-12a, as discussed below.

Following their eruptions, classical and recurrent novae can reach a phase in which coronal lines dominate the spectrum (“the coronal phase”). There are two possible sources for the high degree of ionization needed to produce the coronal lines. One is photoionization by the central white dwarf (WD), whose observed surface temperature after eruption progressively increases until the nova’s pseudo-photosphere reaches the WD surface. During the “super-soft source” (SSS) X-ray phase, the WD surface temperature can reach peak values as high as $100 - 110$ eV, ($[1.16 - 1.27] \times 10^6$ K), and thus become a source of X-rays. The second mechanism for ionization, in the case when the secondary star is a red giant (RG), is shock heating. Mass loss from the RG wind produces an extended envelope of material around the system. During the eruption, the nova’s ejecta, traveling at typically $\sim 1000 - 3000$ km s $^{-1}$, plows into the RG wind creating a strong forward shock and a reverse shock. The shock-heated material can reach temperatures as high as 10^7 K (D. P. K. Banerjee et al. 2014; J. J. Drake et al. 2016). The nova ejecta, impeded by the wind, can decelerate sharply, and a decrease in velocity from $1000 - 3000$ km s $^{-1}$ to a few hundred km s $^{-1}$ is often observed in such systems (e.g., R. Das et al. 2006; U. Munari et al. 2011; D. P. K. Banerjee et al. 2014; A. Evans et al. 2022). The deceleration is inferred from the reduction of the emission line widths with time. Moreover, there can be strong shocks even without a

RG wind, when clumps of nova ejecta collide with each other. Such “internal shocks” have been observed to occur (for example, in nova V959 Mon; L. Chomiuk et al. 2014, 2021).

A. Azzollini et al. (2023, henceforth AA23) have carried out a multi-wavelength spectroscopic study of shock-driven phenomena in the outbursts of symbiotic-like recurrent novae (SyRNe), with an emphasis on RS Ophiuchi. The systems in their study studied included RS Oph itself, V745 Sco, V407 Cyg, and the subject of this paper, V3890 Sgr. AA23 find that, during the eruptions of SyRNe, the line profiles exhibit a broad component that originates in the ejecta and shock, and a narrow component that originates in the RG wind. With regard to the coronal emission, lines such as those of [Fe XI], [Fe XII], [Fe XIV], may appear in post-maximum spectra of SyRNe eruptions. They are strongest in the earliest stages. These lines arise from two separate regions: the ionized wind of the RG (where $T_e \sim 10^4$ K), and the post-shocked ejecta and wind ($T_e > 10^6$ K); the profiles of lines originating in the wind are narrow, while those of lines originating in the post-shock gas are broad (AA23). The presence of [Fe X] $\lambda 6376\text{\AA}$, [Fe XI] $\lambda 7982\text{\AA}$ and [Fe XIV] $\lambda 5303\text{\AA}$ lines in the SyRN V745 Sco is noted, but only the [Fe XI] $\lambda 2648\text{\AA}$ line is reported as being present in V3890 Sgr. We assume the infrared [Fe XIII] $\lambda 10747\text{\AA}$ and $\lambda 10798\text{\AA}$ lines (which were not discussed by AA23 as being present in V3890 Sgr) originate in a similar (or nearby) zone as emission from the higher ionization [Fe XIV] $\lambda 5303\text{\AA}$ line.

1.1. Coronal lines in novae and the Sun

Most of the coronal lines seen in novae are the same as those seen in the solar corona, thereby implying similar physical conditions of temperature and density. Even some of the most highly ionized species, that require photon energies of 285–350 eV to reach the energy levels from which lines such as [Fe XIV] 5303\AA , [Al IX] $2.04\mu\text{m}$, and [Si IX] $1.43\mu\text{m}$ in the infrared, are also routinely seen in novae. This implies that the nova ejecta must be very hot during the coronal stage. However, the [Fe XIII] lines seen in the solar corona have not been identified in nova spectra, the likely reason being that they are intrinsically much weaker than even the wings of the nearby He I 10830\AA line on the redward side, and the strong C I 10690\AA line on the blueward side (the C I line being especially strong in the so-called “Fe II novae”; R. J. Rudy et al. 2000).

The He I 10830\AA is the strongest line in the near-infrared, overwhelming all nearby lines – even the strongest H lines – during the nebular phase. More importantly, its wings can easily extend past the po-

sitions of the Fe XIII lines, since the full width at zero intensity (FWZI) of the He line (or nova lines in general) can reach up to $10,000 \text{ km s}^{-1}$ (e.g., [R. E. Williams 1992](#)). In comparison, the separation between the line centers of the He I 10830Å line and the more distant [Fe XIII] 10757Å line is only $\sim 2030 \text{ km s}^{-1}$. Thus the wings of the He I line can engulf both of the nearby Fe XIII lines. In contrast to this unfavorable situation in novae, in the solar corona the [Fe XIII] and He I lines are narrow and distinctly resolved as separate lines (e.g., Figure 3 of [T. A. Schad et al. 2023](#)). These lines have average full widths at half maximum (FWHM) $< 50 \text{ km s}^{-1}$, as is evident from the consideration that the FWHM of a line due to thermal broadening is $\text{FWHM}_{\text{vel}} = 0.2148 \times (T/M)^{1/2} \text{ km s}^{-1}$, where T is the gas temperature and M is the ion mass in a.m.u. Thus, for Fe XIII and $T = 10^6 \text{ K}$, the $\text{FWHM}_{\text{vel}} \simeq 29 \text{ km s}^{-1}$ for thermal broadening. Observed FWHMs in the solar corona are close to this value.

However, if the secondary in the nova system is a RG and sufficient time has elapsed after eruption for the emission lines to narrow to the order of 100 km s^{-1} , then the [Fe XIII] lines may appear as distinct features in the spectrum. These are the conditions that prevailed when a [Fe XIII] line was detected in the near-infrared spectrum of the extragalactic nova M31-N 2018-12a ([D. P. K. Banerjee et al. 2025](#)). This nova has a RG secondary and its ejecta show a rapid deceleration after outburst. In view of its large distance, the signal from M31-N 2018-12a was weak, even for an 8 m telescope. The Fe XIII detection, which we now believe was a blend of the two [Fe XIII] lines, although not reported as such by [D. P. K. Banerjee et al. \(2025\)](#), appeared genuine, but not so robust as to leave no room for doubt. However, in this paper we show convincing and unambiguous detections of the infrared [Fe XIII] lines in (see Figure 2) the recurrent nova V3890 Sgr.

1.2. The 2019 eruption of V3890 Sgr

Recurrent nova V3890 Sgr underwent eruptions in 1962 and 1990, and had its latest eruption on 2019 Aug 27.87 (JD 2458723.37; [A. Pereira et al. 2019](#)). The system consists of a WD and RG, with masses of $M_{\text{WD}} = 1.35 \pm 0.13 M_{\odot}$ and $M_{\text{RG}} = 1.05 \pm 0.11 M_{\odot}$, respectively ([B. E. Schaefer 2009](#)). Detailed spectroscopic studies of the nova in quiescence and during its 2019 eruption are given in [B. Kaminsky et al. \(2022\)](#) and [A. Evans et al. \(2022\)](#), respectively. During the 2019 outburst, several spectra were obtained by [A. Evans et al. \(2022\)](#) between 5.1 and 46.3 days after the eruption, and used to derive the elemental abundances and esti-

mate the physical parameters and spatio-kinematics of the ejecta.

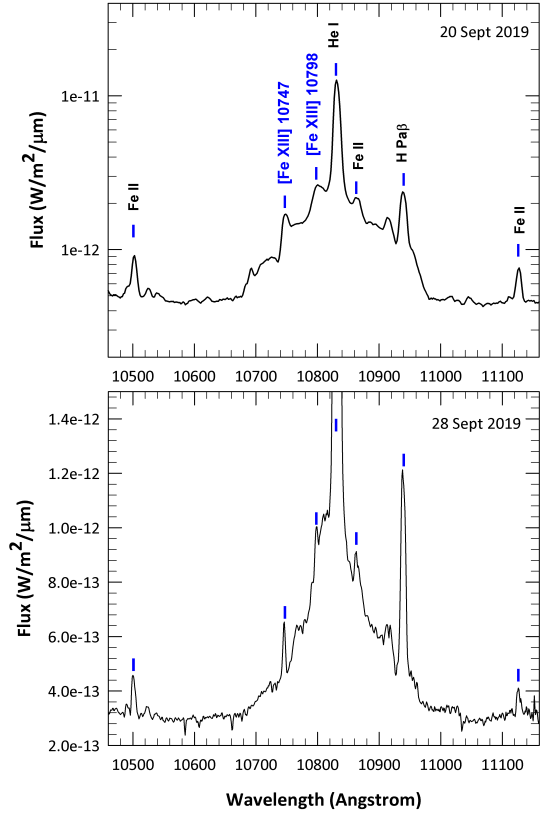


Figure 2. The [Fe XIII] 10747Å, 10798Å forbidden lines, detected at two epochs, against the backdrop of the broad He I 10830Å line. The spectra also clearly reveal Fe II 9997Å (not shown here), 10501, 10863, and 11126Å – the so-called “1 micron Fe II lines” ([R. J. Rudy et al. 2000](#)). These descend from a common upper multiplet and are routinely detected in novae and a variety of emission-line stars. The blue ticks, identifying the lines, are marked at identical wavelengths in both panels. The Y-axis in the bottom panel is on a linear scale to emphasize the weakening of the [Fe XIII] 10798Å line between epochs.

2. RESULTS

2.1. The Infrared [Fe XIII] Lines

We have analyzed the region around the infrared [Fe XIII] lines in two specific spectra, from day 23.43 (spectrum obtained by NASA IRTF /SpeX program 2020A-010) and 31.35 (spectrum obtained by Gemini N/GNIRS for program GN-2019B-DD-104). These are shown in Figure 2. Deceleration of the ejecta was

Table 1. Electron density and temperature from the [Fe XIII] lines.

UT Date	DAO ^a	Facility	Res	Line flux (W m ⁻²) ^b	$\frac{I(10747\text{\AA})}{I(10798\text{\AA})}$	$N_e (\text{cm}^{-3})^c$	$\frac{I(5303\text{\AA})}{I(10747\text{\AA})}$	$\log(T)^d$	$\frac{I(5303\text{\AA})}{I(10798\text{\AA})}$	$\log(T)^e$	
2019-09-20.30	23.43	IRTF	2000	1.04(-15) 8.88(-16) 4.39(-15)	$\frac{I(10747\text{\AA})}{I(10798\text{\AA})}$	1.16-1.35	$\frac{I(5303\text{\AA})}{I(10747\text{\AA})}$	4.23	6.41	4.94	6.40
2019-09-28.22	31.35	GN	6000	1.64(-16) 7.12(-17) 3.95(-16)	$\frac{I(10747\text{\AA})}{I(10798\text{\AA})}$	2.30	$\frac{I(5303\text{\AA})}{I(10747\text{\AA})}$	2.41	6.38	5.55	6.39

NOTE—^aDays after outburst, with t_0 taken as 2019 Aug 27.87 (JD 2458723.37; Pereira 2019). ^bLine fluxes are dereddened using $E(B - V) = 0.5$ from Evans et al. (2022). $X(\pm YY)$ denotes $X \times 10^{\pm YY}$ for both line fluxes and electron density. ^cElectron density estimated using tabular and other data in Chevalier & Lambert (1969) and Malville (1967). ^d $\log(T)$ computed from the $I(5303\text{\AA})/I(10747\text{\AA})$ ratio using Srivastava et al. (2007). ^e $\log(T)$ computed from the $I(5303\text{\AA})/I(10798\text{\AA})$ ratio using Srivastava et al. (2007). ^fThe mean temperature for the [Fe XIII] lines on Sep 20 and 28 is $\log(T) = 6.4 \pm 0.01$ ($T = 2.51 \times 10^6$ K).

rapid in V3830 Sgr, and by days 23.43 and 31.35, the FWHMs of the lines, deconvolved for instrumental broadening, had decreased to 305 km s^{-1} and 230 km s^{-1} , respectively. In contrast, on Aug 28.895 (one day after the outburst) $\text{H}\alpha$, based on data from the ARAS² database (F. Teyssier 2019), reveal that the $\text{H}\alpha$ line had a FWHM of $\sim 5400\text{ km s}^{-1}$. The deceleration implies that a strong shock had developed in the system. Coronal lines developed early, those observed in the near-infrared and their evolution are given in A. Evans et al. (2022). Based on the short duration of the SSS phase, which had ended by day 26, A. Evans et al. (2022) proposed that the ions producing the coronal emission in the later spectra (> 23 days) were solely collisionally ionized and excited.

Figure 2 shows the principal lines seen, with their rest wavelengths in air denoted by blue tick-marks. The [Fe XIII] lines are clearly seen at both epochs. Apart from $\text{He I } 10\,830\text{\AA}$ and hydrogen $\text{P}\gamma$, several “1 micron Fe II lines” are also seen, some details of which are given in the caption of Figure 2. The results of the analysis of the line ratios are presented in Table 1. The observed line flux ratios, $I(10\,747\text{\AA})/I(10\,798\text{\AA})$, listed in Table 1, were compared with theoretical predictions using tabular and graphical data from three independent studies, including those of J. McKim Malville (1967), R. A. Chevalier & D. L. Lambert (1969), and J. Dudík et al. (2021).

2.2. The Infrared [Fe XIII] Lines and Electron Density

AA23 used the flux ratio

$$r = \frac{f(\text{Si III]} \lambda 1892\text{\AA})}{f(\text{C III]} \lambda 1909\text{\AA})} \quad (1)$$

obtained from low resolution IUE and Swift grism data, to estimate the electron density. Their Figure 15 suggests that this ratio is reasonably consistent over the 1990 and 2019 eruptions.

Using the infrared [Fe XIII] lines, we determine the electron density (N_e) to be $\sim 10^{10}\text{ cm}^{-3}$ on day 23.43 of the 2019 eruption, see Figure 3. AA23 obtained $1.74 \times 10^9\text{ cm}^{-3}$ and $1.63 \times 10^9\text{ cm}^{-3}$ respectively for days 19 and 27 using low resolution IUE spectra (1990 outburst of V3890 Sgr), and $3.21 \times 10^9\text{ cm}^{-3}$ on day 21.5 from Swift grism data (2019 outburst). Despite the large difference in the ionization states of the infrared lines used here and the IUE and Swift lines used by them to determine N_e , our values are in reasonable agreement.

² <https://aras-database.github.io/database/novae.html>

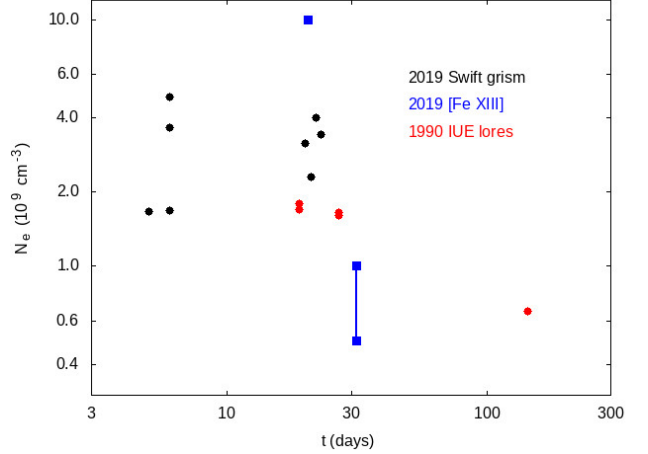


Figure 3. Variation of the electron density (N_e) for V3890 Sgr from A. Azzollini et al. (2023); their values were binned and averaged over intervals of 2 days. The blue squares correspond to data from this infrared study. See Table 1 and text (section 2.2) for details.

To determine the temperature, we used the analysis of A. K. Srivastava et al. (2007), which compares the ratio of the two [Fe XIII] lines with the 5303\AA line. For the 5303\AA flux, we used flux-calibrated, high-resolution spectra on 2019 Sept 20.04UT and 26.014UT from the SMARTS database³ (F. M. Walter et al. 2012). These were the closest in time to our spectra presented in Figure 2. The four values of the gas temperature, derived on both days and from both ratios $I(5\,303\text{\AA})/I(10\,757\text{\AA})$ and $I(5\,303\text{\AA})/I(10\,798\text{\AA})$, are very similar and lie in the range $\log T = 6.38 - 6.41$. These are indicated in Table 1; the mean temperature of the four measurements is $\log T = 6.40 \pm 0.01$ K ($T = [2.51 \pm 0.06] \times 10^6$ K). In comparison, A. Evans et al. (2022), using ratios of line fluxes from different sets of coronal lines of sulphur and silicon, get an average value of $\log T = 5.97 \pm 0.11$, or $T = 9.3^{+2.7}_{-2.1} \times 10^5$ K on day 23.43 (September 20.30). The highest temperature obtained by them for that day is $\log T = 6.17$ by using lines of [S IX] and [S XII]. The derived temperature here is in reasonable agreement with values in A. Evans et al. (2022).

It is puzzling why the density dropped by a factor exceeding 10 between day ~ 23 to ~ 31 . (Table 1 shows a change from 10^{10} cm^{-3} to $10^{8.5-9}\text{ cm}^{-3}$ in the ~ 8 day period between day 23.43 and 31.35). The drop is not an artifact of the analysis. Visual examination of Figure 2 shows convincingly how much weaker the $10\,798\text{\AA}$ line has become in the second epoch, boosting $I(10\,747\text{\AA})/I(10\,798\text{\AA})$ by almost a factor of two

³ <https://www.astro.sunysb.edu/fwalter/SMARTS/NovaAtlas/>

between epochs. For the Sun, a decrease in density with distance from the limb leads to higher values of $I(10747\text{\AA})/I(10798\text{\AA})$. As examples, see Figures 2 of [J. McKim Malville \(1967\)](#) and [J. Dudík et al. \(2021\)](#), and Table IV of [R. A. Chevalier & D. L. Lambert \(1969\)](#). However, if a decrease in the density of the ejecta occurred due solely to its expansion at constant velocity, it would be by a factor of $1.8 = (31.35/23.43)^2$ between the 2 epochs if the dilution is geometric ($N_e \propto r^{-2}$, or equivalently $N_e \propto t^{-2}$). If the dilution is steeper (e.g., $N_e \propto r^{-3}$; [P. H. Hauschildt et al. 1992, 1997](#)), then the density would have decreased by a factor of 2.4. But this still does not explain the observed data which shows a larger decrease in density. Indeed, the observed decrease in N_e requires that the decline must be at least as steep as t^{-8} , which seems unreasonable.

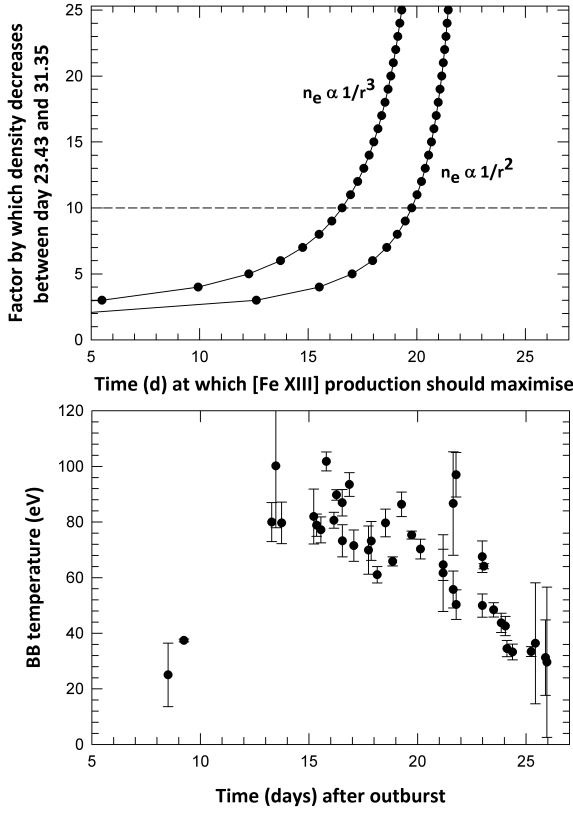


Figure 4. The continuous lines show the time at which the bulk of the [Fe XIII] should be produced to explain the drop in density of the ejecta by a factor of 10 or more in 8 days. The dashed line gives an example that a drop in density by 10, requires that the [Fe XIII] ion production maximize at around day 16 (for $N_e \propto r^{-3}$ expansion law). The bottom panel, based on Swift observations, shows the evolution of the black body temperature of the white dwarf during the SSS phase (see Section 2.2, as well as [K. L. Page et al. \(2020\)](#)).

An alternative explanation for this behavior could be the following. We suppose that the [Fe XIII] production maximized on some day t_{XIII} (< 23.43 days) after outburst. If the dilution of the ejecta follows the form $N_e \propto r^{-n}$, then to account for an increase by a factor $\alpha \simeq 10 - 25$ in the $I(10757\text{\AA})/I(10798\text{\AA})$ ratio between days 23.43 to day 31.35, the following equation should hold

$$[(31.35 - t_{\text{XIII}})/(23.43 - t_{\text{XIII}})]^n = \alpha . \quad (2)$$

This is solved for t_{XIII} and the solution is plotted in Figure 4 for values of $n = 2, 3$. It is seen that for $n = 3$, the density will decrease by a factor of 10 (as is close to what is observed) if most of the [Fe XIII] ions are produced on day 16.65. The blackbody temperature, derived from the super soft X-ray emission, also peaked near day 16 at ~ 101.8 eV (see Figure 4 (bottom)) after the onset of the SSS phase. A value of $n = 3$ is frequently used in CLOUDY (e.g., [C. M. Gunasekera et al. 2025](#)) modeling, and may correspond to a homologous flow ([P. H. Hauschildt et al. 1992, 1997](#)).

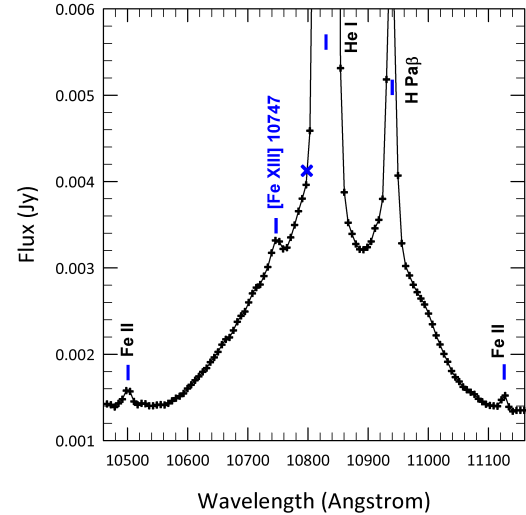


Figure 5. The [Fe XIII] 10747 \AA line in SN 1987A. This figure was prepared using JWST/NIRSPEC data available from the Mikulski Archive (MAST). The original study is described in [J. Larsson et al. \(2023\)](#), who found several high-ionization coronal lines from the equatorial ring of SN 1987A, requiring a temperature $\geq 2 \times 10^6$ K. As in Figure 2, we identify two of the “1 micron Fe lines” here to show the similarity with the profile in V3890 Sgr. A blue “X” shows the expected position of the 10798 \AA Fe line, which however is not seen. The observed spectrum had to be shifted blueward by 13 \AA to make the H, He and Fe II spectral features match with their rest wavelengths.

3. DISCUSSION AND CONCLUSION

Apart from the 10747Å and 10798Å lines, it is also possible to search in novae for the 3388Å line (see the term diagram in Figure 1). However, detection of that line should be challenging; it is accessible from the ground from a few observing sites, but also it is intrinsically weak, about one-fifth of the 10757Å line in intensity (R. A. Chevalier & D. L. Lambert 1969). It is a useful alternative as a density diagnostic, as can be seen from the data in R. A. Chevalier & D. L. Lambert (1969), where the predicted ratios of 3388Å relative to [Fe XIII] infrared lines are listed over a range of densities and temperatures. The line can be covered, for example, by the ultraviolet and visible grisms onboard a facility such as Swift, and can be observed from the ground, for example from the Sutherland site of the South African Astronomical Observatory (K. H. Nordsieck et al. 2001).

To obtain supplementary support for our detections of the [Fe XIII] lines here, we have searched for detections by others. It transpires that there are very few instances where the [Fe XIII] lines have been detected. Among them, the 10747Å line was reported in the symbiotic star R Aqr (H. Zirin 1976), but the image was recorded on photographic plates and is not available for inspection. The 10798Å line is neither seen nor marked on the photographic plate.

This study shows that the likelihood of making more detections of the [Fe XIII] lines in other novae will be higher under the following conditions: (a) the nova should have a giant secondary with a wind to decelerate the nova ejecta leading to the narrowing of emission lines, which could occur in a recurrent nova or even a symbiotic nova (e.g., V407 Cyg; D. P. K. Banerjee et al. 2014) with a RG/Mira secondary; (b) the nova should be in the coronal stage; (c) the lines should have narrowed sufficiently that the [Fe XIII] lines stand out sharply and distinctly even if they are on the wings of a much-stronger He I 10830Å line; and (d) intermediate ($R > 2000$) or higher resolution is available to allow the lines to stand out and thus facilitate detection.

In this context, the recurrent nova T CrB, which has a RG secondary, seems to be a suitable and attractive candidate. T CrB is expected to erupt imminently. Its outburst is keenly awaited by the astronomical community because it erupts only once every 80 years – its last outburst was in 1946. It has a mysterious second maximum in the visual light curve, and also displays an uncommon phenomenon of its spectrum switching from the He/N to Fe II class during its evolution (see W. W. Morgan & A. J. Deutsch 1947). Since the infrared [Fe XIII] lines are very sensitive density indicators, they could give use-

ful information on T CrB (and other systems) if these lines are detected in its spectrum.

ACKNOWLEDGMENTS

The authors wish to thanks the prompt and insightful comments of the referee that improved this manuscript.

The IRTF data presented in this paper were obtained partly under IRTF program 2020A-010. The Infrared Telescope Facility is operated by the University of Hawaii under contract 80HGTR19D0030 with the National Aeronautics and Space Administration. The Gemini observations were made possible by awards of Director's Discretionary Time for program GN-2019B-DD-104. The international Gemini Observatory is a program of NSF's NOIRLab, which is managed by the Association of Universities for Research in Astronomy (AURA) under a cooperative agreement with the National Science Foundation, on behalf of the Gemini Observatory partnership: the National Science Foundation (United States), National Research Council (Canada), Agencia Nacional de Investigación y Desarrollo (Chile), Ministerio de Ciencia, Tecnología e Innovación (Argentina), Ministério da Ciência, Tecnologia, Inovações e Comunicações (Brazil), and Korea Astronomy and Space Science Institute (Republic of Korea).

This work is based in part on observations made with the NASA/ESA/CSA James Webb Space Telescope. The data were obtained from the Mikulski Archive for Space Telescopes at the Space Telescope Science Institute, which is operated by the Association of Universities for Research in Astronomy, Inc., under NASA contract NAS 5-03127 for JWST. These observations are associated with program #1726 and can be accessed via doi 10.17909/175h-7x33.

SS acknowledges partial support from a NASA Emerging Worlds grant to ASU (80NSSC22K0361) as well as support from his ASU Regents' Professorship. CEW acknowledges partial support from NASA grant JWST-GO-01731.006-A. We acknowledge the use of the SMARTS database and also thank Umberto Sollecchia who obtained the ARAS spectra used here.

Facilities: Gemini:Gillett (GNIRS), IRTF (SpeX), JWST

REFERENCES

Azzollini, A., Shore, S. N., Kuin, P., & Page, K. L. 2023, *A&A*, 674, A139, doi: [10.1051/0004-6361/202245185](https://doi.org/10.1051/0004-6361/202245185)

Banerjee, D. P. K., Geballe, T. R., Evans, A., et al. 2025, *MNRAS*, 540, 1780, doi: [10.1093/mnras/staf817](https://doi.org/10.1093/mnras/staf817)

Banerjee, D. P. K., Joshi, V., Venkataraman, V., et al. 2014, *ApJL*, 785, L11, doi: [10.1088/2041-8205/785/1/L11](https://doi.org/10.1088/2041-8205/785/1/L11)

Chevalier, R. A., & Lambert, D. L. 1969, *SoPh*, 10, 115, doi: [10.1007/BF00146161](https://doi.org/10.1007/BF00146161)

Chomiuk, L., Metzger, B. D., & Shen, K. J. 2021, *ARA&A*, 59, 391, doi: [10.1146/annurev-astro-112420-114502](https://doi.org/10.1146/annurev-astro-112420-114502)

Chomiuk, L., Linford, J. D., Yang, J., et al. 2014, *Nature*, 514, 339, doi: [10.1038/nature13773](https://doi.org/10.1038/nature13773)

Das, R., Banerjee, D. P. K., & Ashok, N. M. 2006, *ApJL*, 653, L141, doi: [10.1086/510674](https://doi.org/10.1086/510674)

Drake, J. J., Delgado, L., Laming, J. M., et al. 2016, *ApJ*, 825, 95, doi: [10.3847/0004-637X/825/2/95](https://doi.org/10.3847/0004-637X/825/2/95)

Dudík, J., Del Zanna, G., Rybák, J., et al. 2021, *ApJ*, 906, 118, doi: [10.3847/1538-4357/abcd91](https://doi.org/10.3847/1538-4357/abcd91)

Edlén, B. 1945, *MNRAS*, 105, 323, doi: [10.1093/mnras/105.6.323](https://doi.org/10.1093/mnras/105.6.323)

Evans, A., Geballe, T. R., Woodward, C. E., et al. 2022, *MNRAS*, 517, 6077, doi: [10.1093/mnras/stac2363](https://doi.org/10.1093/mnras/stac2363)

Gunasekera, C. M., van Hoof, P. A. M., Dehghanian, M., et al. 2025, arXiv e-prints, arXiv:2508.01102, doi: [10.48550/arXiv.2508.01102](https://doi.org/10.48550/arXiv.2508.01102)

Hauschildt, P. H., Shore, S. N., Schwarz, G. J., et al. 1997, *ApJ*, 490, 803, doi: [10.1086/304904](https://doi.org/10.1086/304904)

Hauschildt, P. H., Wehrse, R., Starrfield, S., & Shaviv, G. 1992, *ApJ*, 393, 307, doi: [10.1086/171507](https://doi.org/10.1086/171507)

Kaminsky, B., Evans, A., Pavlenko, Y. V., et al. 2022, *MNRAS*, 517, 6064, doi: [10.1093/mnras/stac2199](https://doi.org/10.1093/mnras/stac2199)

Larsson, J., Fransson, C., Sargent, B., et al. 2023, *ApJL*, 949, L27, doi: [10.3847/2041-8213/acd555](https://doi.org/10.3847/2041-8213/acd555)

Lyot, B. 1939, *MNRAS*, 99, 580, doi: [10.1093/mnras/99.8.580](https://doi.org/10.1093/mnras/99.8.580)

McKim Malville, J. 1967, *ApJ*, 148, 229, doi: [10.1086/149139](https://doi.org/10.1086/149139)

Morgan, W. W., & Deutsch, A. J. 1947, *ApJ*, 106, 362, doi: [10.1086/144972](https://doi.org/10.1086/144972)

Munari, U., Joshi, V. H., Ashok, N. M., et al. 2011, *MNRAS*, 410, L52, doi: [10.1111/j.1745-3933.2010.00979.x](https://doi.org/10.1111/j.1745-3933.2010.00979.x)

Nordsieck, K. H., Burgh, E. B., Kobulnicky, H. A., et al. 2001, in American Astronomical Society Meeting Abstracts, Vol. 199, American Astronomical Society Meeting Abstracts, 102.04

Page, K. L., Kuin, N. P. M., Beardmore, A. P., et al. 2020, *MNRAS*, 499, 4814, doi: [10.1093/mnras/staa3083](https://doi.org/10.1093/mnras/staa3083)

Pereira, A., Waagen, E. O., & Pearce, A. 2019, Central Bureau Electronic Telegrams, 4660, 1

Rudy, R. J., Mazuk, S., Puetter, R. C., & Hamann, F. 2000, *ApJ*, 539, 166, doi: [10.1086/309222](https://doi.org/10.1086/309222)

Schad, T. A., Kuhn, J. R., Fehlmann, A., et al. 2023, *ApJ*, 943, 59, doi: [10.3847/1538-4357/acabbd](https://doi.org/10.3847/1538-4357/acabbd)

Schaefer, B. E. 2009, *ApJ*, 697, 721, doi: [10.1088/0004-637X/697/1/721](https://doi.org/10.1088/0004-637X/697/1/721)

Srivastava, A. K., Singh, J., Dwivedi, B. N., et al. 2007, *Bulletin of the Astronomical Society of India*, 35, 457

Teyssier, F. 2019, *Contributions of the Astronomical Observatory Skalnate Pleso*, 49, 217

Walter, F. M., Battisti, A., Towers, S. E., Bond, H. E., & Stringfellow, G. S. 2012, *PASP*, 124, 1057, doi: [10.1086/668404](https://doi.org/10.1086/668404)

Williams, R. E. 1992, *AJ*, 104, 725, doi: [10.1086/116268](https://doi.org/10.1086/116268)

Zirin, H. 1976, *Nature*, 259, 466, doi: [10.1038/259466a0](https://doi.org/10.1038/259466a0)